ingegneria sismica
International Journal of Earthquake Engineering
Anno XLIII - Num. 1 - 2026

Design of Intelligent Generation Algorithm for 500kV Substation Main Wiring Scheme Based on Large Language Modeling

Yuwei Li[1], *Jinghe Zhang*[1], *Feng Lan*[1], *Mingshu Zhao*[2] *and Yi Luo*[2,*]

[1] Economic & Technology Research Institute, State Grid Shandong Electric Power Company, Jinan, Shandong, 250000, China
[2] Institute of Energy Sensing and Information, Tsinghua Sichuan Energy Internet Research Institute, Chengdu, Sichuan, 610000, China

SUMMARY: *As regional hub substations, the main busbar configurations of 500kV substations critically impact grid reliability and economic efficiency. To address this, this paper designs an intelligent design support system for substation main busbar schemes enhanced by vector retrieval based on large language models. The set-pair analysis method is introduced to assess the risks of main busbar configurations, which are then combined with quantitative economic indicators to form multidimensional data. Building upon this foundation, principal component analysis (PCA) is applied to comprehensively evaluate the multidimensional data indicators, ultimately determining the most optimal main busbar configuration. Experimental results demonstrate that the large language model, trained on a knowledge base of 500kV substation main busbar configurations, exhibits outstanding performance in long-text generation, achieving a maximum ROUGE-L score of 0.9876. Furthermore, the comprehensive evaluation method based on PCA further validates the effectiveness of the proposed design methodology. This research addresses the power industry's demand for efficient, intelligent substation main busbar configuration design support.*

KEYWORDS: *Large Language Model; 500kV Substation Main Busbar Configuration; Vector Retrieval Enhancement; Sequential Monte Carlo Model; Principal Component Analysis*

1 Introduction

The primary busbar arrangement of a 500kV substation is a critical component responsible for power transformation and distribution. It significantly influences the selection and layout of electrical equipment, determining system operational flexibility, maintenance accessibility, and economic rationality [1-3]. Different primary busbar configurations for electrical equipment exhibit distinct advantages and disadvantages in operational reliability, flexibility, and economic efficiency. The selection of primary busbar arrangements and the rational configuration of relay protection systems critically impact the secure and stable operation of power grids [4, 5]. Based on the specific operational requirements for reliability and flexibility at different substations, along with the actual conditions in substation planning, various primary busbar configurations and operational modes can be chosen.

With accumulated experience in substation planning, design, and operation, the selection of primary electrical main wiring configurations is increasingly standardized. This trend greatly facilitates substation operation, maintenance, and management, as well as the standardized

*luoyi678@163.com
https://doi.org/10.65102/is2026097 Published: 30 April, 2026

configuration of relay protection, offering significant advantages for newly commissioned substations [6-8]. However, blindly pursuing standardization while ignoring actual conditions may lead to adverse effects such as extended project timelines, expanded power outage areas, and increased construction risks. Moreover, optimized solutions tailored to specific site conditions in original substation designs may be lost [9]. Therefore, the rationality and reliability of main wiring schemes are critically important for the power system, whether for newly commissioned or existing substations.

Against the backdrop of grid digital transformation and intelligent equipment development, the limitations of traditional main wiring design—relying on designer experience and specification manuals—have become glaringly apparent. These include prolonged design cycles, difficulties in handling complex operational scenarios, and poor adaptability of design solutions. Consequently, the intelligent generation of main wiring schemes has become an urgent necessity [10, 11]. Reference [12] proposes an algorithm for automatically generating distribution device schemes for step-down transformers in 6-10kV substations. Based on technical specifications and design decisions, this algorithm enables automatic generation, import, and editable graphic format conversion of substation switchgear electrical connections, reducing project documentation creation time. Reference [13] constructs a layout optimization objective function based on substation SSD files, considering busbar length and layout uniformity. It incorporates a simulated annealing algorithm to reduce layout optimization iterations, achieving main busbar diagram generation through cooling schedules and iterative optimization. Reference [14] employs image recognition and optical character recognition to detect fundamental elements, topological connections, and equipment names within substation image files. It generates corresponding CIM/G files and uses natural language processing to associate basic elements with model data, automatically producing CIM/G diagrams for primary substation wiring diagrams. Reference [15] employs three styles based on substation graphic standards (layout, container, and graphic) for style instantiation and arrangement, providing an intelligent generation method for main and sub-schematics to enhance work efficiency. Reference [16] combines voltage levels, wiring types, and equipment sequence steps. Assisted by the YOLOv5 algorithm, it identifies substation main wiring diagrams. A tree-based classification method effectively compensates for small target recognition discrepancies and wiring relationship classification differences, thereby extracting key information between main wiring diagrams. Reference [17] constructs a graph structure model of substation main wiring diagrams using the Neo4j knowledge graph. Combined with real-time interaction via Deep Q-Network duels, it automatically learns substation operation sequences, enabling correct operational sequences under various wiring schemes.

Large Language Models (LLMs) represent a deep learning-based natural language processing technology. Their primary objective is to enable computers to understand and generate natural language through massive training datasets and powerful computational capabilities [18]. With rapid advancements in deep learning, LLMs have achieved significant breakthroughs in natural language processing, machine translation, and text generation [19]. Particularly in text generation, LLMs demonstrate immense potential through their capabilities in unstructured text processing, cross-domain knowledge transfer, multimodal data fusion, and natural language interaction, paving the way for intelligent generation of main connection schemes [20-23]. Currently, LLM applications have extended into the power industry. Reference [24] highlights that LLMs excel in data generalization and multimodal data management for smart grids. They optimize human-machine interaction, making grid operations more convenient and intuitive, while enhancing system security and privacy. LLMs also provide solutions for system compatibility and integration challenges. Reference [25] establishes an LLM-based adaptive optimization framework for intelligent microgrid self-

healing, addressing dynamic fault propagation and multimodal data fusion challenges in traditional power systems. Reference [26] employs LLMs to augment power network structural data, explore grid internal structures, and generate power structure images using visualization techniques, thereby optimizing the generation, verification, and visualization processes for small-scale power grids.

Relying on existing technologies struggles to meet the demands for high automation and accuracy in future intelligent power system design support. To address these challenges, this paper proposes an intelligent generation model for 500kV substation main busbar schemes based on large language models. By integrating vector retrieval and natural language generation techniques, it achieves efficient retrieval of main busbar information and personalized scheme generation. Additionally, it employs set-wise principal component analysis for comprehensive evaluation of generated schemes. First, a domain-specific knowledge vector library is constructed by encoding power equipment and selection knowledge into high-dimensional vectors, enabling precise and rapid knowledge retrieval. Second, group query attention and dual-block attention mechanisms are introduced to optimize multi-round retrieval processes. Relevant knowledge is swiftly located by calculating similarity between user requirements and knowledge base vectors. Furthermore, prompt engineering and large language models are employed for multi-turn dialogue and context tracking, dynamically generating selection solutions that meet user requirements, thereby enhancing the system's intelligence. Finally, the reliability metrics of main busbar configurations are quantitatively assessed using set-pair analysis. Subsequently, economic metrics are integrated, and principal component analysis is applied to evaluate and determine the most optimal main busbar configuration, followed by experimental analysis based on this outcome.

2 Intelligent Generation Model for Main Busbar Schemes of 500kV Substations

2.1 Large Language Models

2.1.1 Central Language Model

Before constructing the design support system, considering the confidentiality of power grid-related data, an open-source large language model was selected for deployment to ensure data remains stored locally, thereby guaranteeing overall security. To guarantee retrieval and interaction efficiency, the CompassArena ranking was referenced to match models against task requirements. The open-source GPT-3.5-Turbo and ChatGLM2-6B large language models were selected as the foundation for vector retrieval enhancement and the core language models for the system. Figure 1 illustrates the large language model question-answering architecture under vector retrieval enhancement.

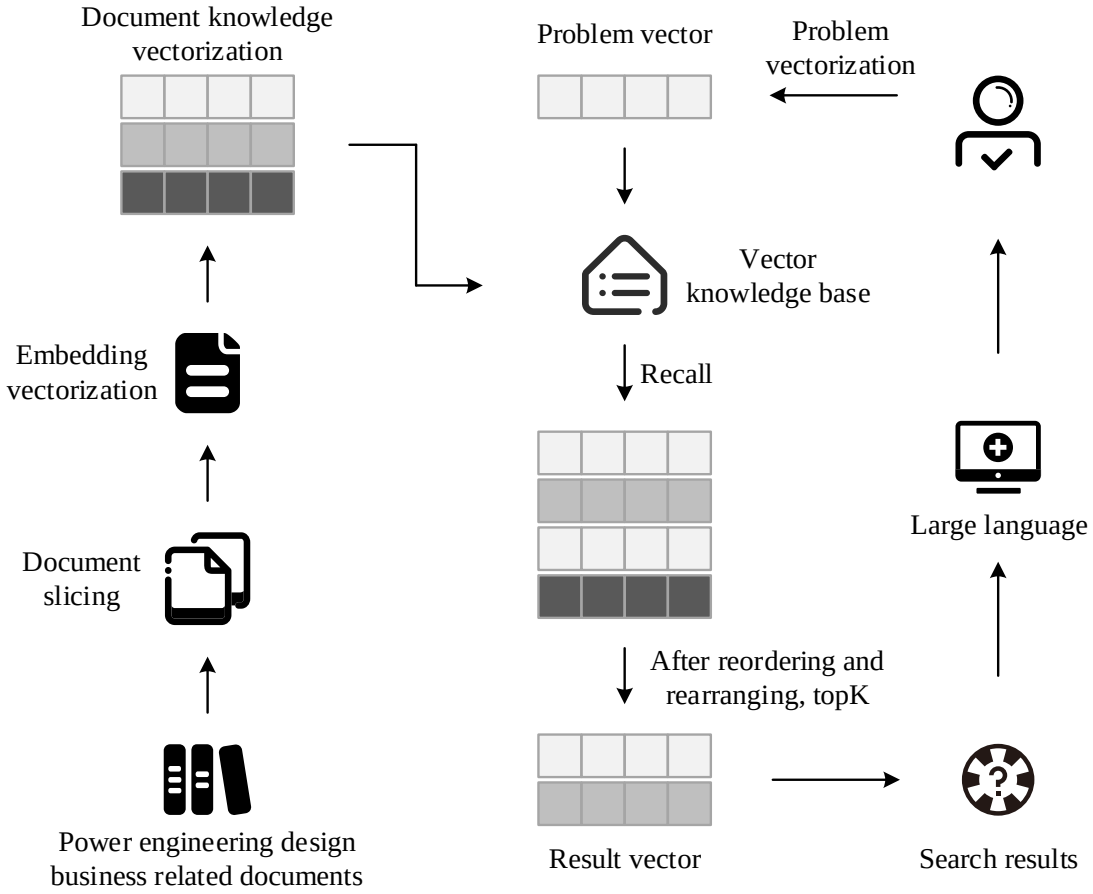

Figure 1: The large language q&a structure of the vector enhancement retrieval

2.1.2 Group Query Attention Mechanism and Block Attention Mechanism

Large language models typically adopt the Transformer architecture, but inference and generation efficiency vary significantly across different models. To further optimize the selection efficiency of the model selection system, the Grouped Query Attention (GQA) mechanism was employed. By reducing the use of key-value caching, this approach significantly improved inference efficiency. This mechanism enables the system to compute more effectively and reduce inference latency when handling long contexts. Self-attention calculations are performed using Equation (1):

$$f_{Att}(Q,K,V) = \sigma(\frac{QK^T}{\sqrt{d_k}})V \tag{1}$$

In the equation, Q is the query matrix, representing the query portion of the input data used to compute attention weights. K represents the key matrix, denoting the key portion of the input data, which participates in attention score calculation alongside the query matrix. V represents the value matrix, denoting the value portion of the input data, where attention scores are applied to generate the output. σ denotes the softmax function, and d_k denotes the dimension of the k th key.

Within the self-attention mechanism, these matrices determine the weighting of information in the value matrix V by calculating the similarity between the query matrix Q and the key matrix K, thereby generating the final output.

Additionally, the main busbar connection methods in 500kV substations often involve extensive historical data and long-term sequence information, necessitating in-depth analysis of correlations between multiple events. To handle ultra-long contexts, the system introduces a Dual-Block Attention (DCA) mechanism. This approach decomposes long sequences into multiple blocks while establishing more precise dependencies between them. This technique effectively expands the context window, ensuring the model captures greater detail when processing long-time-series data. DCA maintains consistent dependencies within each block by processing long sequences in chunks, transferring information across blocks via Equation (2):

$$F_{DCA}(X) = \sum_{i=1}^{n} f_{Att}(X_i, X_j) \tag{2}$$

In the equation, X_i, X_j represent different blocks, with information integrated through cross-block attention mechanisms. This long-range context processing capability makes the system particularly well-suited for analyzing complex equipment selection requirements. Figure 2 shows the detailed results of DCA.

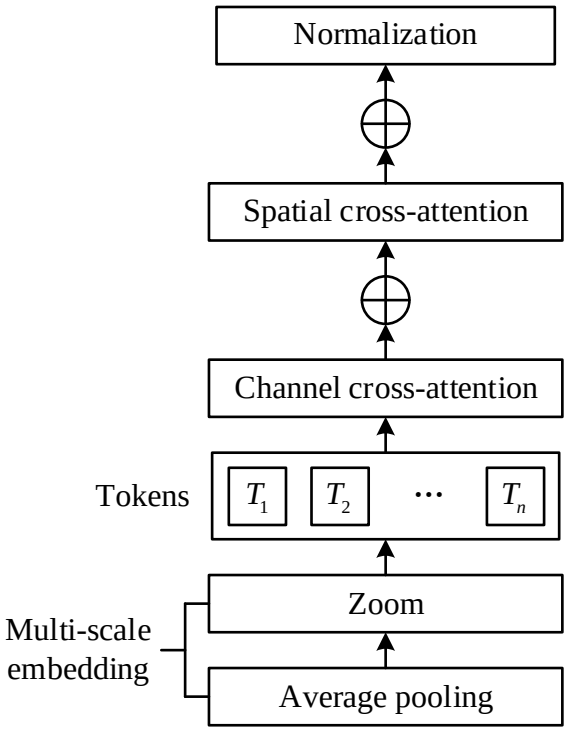

Figure 2: Double attention mechanism

2.1.3 Vector Retrieval-Augmented Generation

To enhance retrieval efficiency, the system employs vector retrieval-enhanced generation technology. First, detailed requirement scenarios for main busbar selection at 500kV substations are vectorized. Cosine similarity is then calculated using Equation (3) to match historical busbar configuration cases. That is:

$$D_{Sim}(x, x_i) = \frac{v_x \cdot v_{x_i}}{\| v_x \| \| v_{x_i} \|} \tag{3}$$

In the equation, $v_x \cdot v_{x_i}$ denotes the dot product (inner product) of v_{x_i} and v_{x_i}, The dot product is the sum of the products of corresponding positions of two vectors, representing their similarity to some extent.

Then, based on the retrieval results, the system generates selection analysis and recommendations through its generation capability. This process can be further optimized to generate multiple selection recommendations and calculate the conditional probability using Equation (4) to select the optimal result:

$$P(y \mid x') = \prod_{t=1}^{T} P(y_t \mid y_{<t}, x') \tag{4}$$

In the formula: $P(y \mid x^{'})$ denotes the joint probability of the output sequence y given the input $x^{'}$. Here, y represents the target output sequence (e.g., model selection recommendation text), while $x^{'}$ denotes the input conditions (e.g., user requirements, product parameters, etc.), expressed after preprocessing or encoding. T denotes the length of the input sequence (i.e., the total number of generated symbols), y_t represents the symbol at the t th position in the output sequence (e.g., the t th word or character), $y < t$ denotes the sequence of the first $t-1$ symbols (i.e., $y_1, y_2, \cdots, y_{t-1}$), representing the partially generated content during the generation process.

2.2 Intelligent Analysis Process for Main Busbar Schemes of 500kV Substations

In the intelligent analysis of main busbar configurations for 500kV substations, real-time performance and accuracy are paramount. Utilizing vector retrieval technology, the system efficiently extracts configuration options from an extensive historical database that closely match user requirements. This retrieval technique integrates natural language processing to parse user-input equipment selection criteria and convert them into high-dimensional vector representations.

The system generates a vector based on the user's natural language selection requirements, then retrieves the database using Equation (5) to perform vector similarity matching:

$$x' = \alpha D_{Sim}(x, x_i) \tag{5}$$

In the equation, x represents the database content, x_t denotes the updated context based on the user's input in the current dialogue round, and x' signifies the result obtained through vector similarity retrieval.

Through this context tracking mechanism, the system can progressively refine model selection recommendations across multi-turn dialogues, enhancing the accuracy of the final generated results. α denotes the argmax function.

Through this context tracking mechanism, the system progressively refines selection recommendations across multiple dialogue rounds, enhancing the accuracy of final generated results. Integrating domain-specific knowledge bases effectively suppresses model hallucinations, while combining multi-turn dialogue memory further improves response accuracy. This enables the construction of a reliable, automated 500kV substation main busbar configuration generation system.

3 Evaluation Model for Generating Main Connection Schemes of 500kV Substations

3.1 Risk Assessment of Main Busbar Connections in Substations Based on Set Pair Analysis

3.1.1 Substation Main Connection Connectivity Analysis

The core issue in assessing the risk of a substation's main connection is analyzing whether a failure of internal components or a combination of component failures could cause an interruption in the substation's incoming and outgoing lines. The connectivity analysis process for the main connection in this paper is as follows: First, establish the adjacency matrix of the substation's main connection. Based on this, form the affected outage matrix for internal components. By sampling the substation system state using the Monte Carlo method and applying logical operations, the reachability matrix is obtained, thereby determining the system's connectivity under that state.

(1) Consequential Outage Matrix

When an extensive fault occurs within a substation's internal components, adjacent circuit breakers trip to isolate the faulty element. If these adjacent circuit breakers also fail, the impact of the fault will further expand.

Therefore, it is necessary to establish a cascading outage matrix to determine the scope of impact when a main switching element fails at a substation. The cascading outage matrix is represented with the failed element p as rows and the cascading outage elements q as columns, as shown in its matrix expression (6):

$$O = \begin{bmatrix} o_{11} & o_{12} & \cdots & o_{1h} \\ o_{21} & o_{22} & \cdots & o_{2h} \\ \vdots & \vdots & \vdots & \vdots \\ o_{h1} & o_{h2} & \cdots & o_{hh} \end{bmatrix}_{h\times h} \tag{6}$$

In the formula, o_{pq} represents the tripping factor. $o_{pq}=1$ indicates that the extended fault of element p causes element q to be tripped, while $o_{pq}=0$ indicates that the extended fault of element p has no effect on element q.

(2) Reachability Matrix

After establishing the substation main connection adjacency matrix and the internal component cascading outage matrix, the reachability matrix can be derived using logical operations to perform connectivity analysis on the main connection. Let the reachability matrix be $D=(d_{xy})_{g\times g}$, calculated as follows: First, compute the powers of the adjacency matrix B: $B_1, B_2, \cdots, B_g$. Then, using logical operations, the reachability matrix of the substation main busbar configuration can be obtained as $D = B_1 \vee B_2 \vee \cdots \vee B_g$.

The reachability matrix determines connectivity between any two nodes in the substation main connection. $d_{xy}=1$ indicates nodes v_x and v_y are connected, while $d_{xy}=0$ indicates nodes v_x and v_y are disconnected.

3.1.2 Monte Carlo Sampling

The non-sequential Monte Carlo simulation method is independent of the number of samples and system scale, offering advantages such as rapid convergence [27]. The state of each component can be obtained by sampling the probability of the component being in that state. Taking a transformer as an example, let P_N, P_M, P_S denote the probabilities of the transformer being in normal state, planned maintenance state, and extended fault state, respectively. Let s_r represent the state of the r th transformer. Generate a random number R_r uniformly distributed in the interval [0, 1]. That is:

$$s_r = \begin{cases} 0, & 0 \le R_r \le P_N \\ 1, & P_N < R_r \le P_S \\ 2, & P_S < R_r \le P_S + P_N + P_M \end{cases} \tag{7}$$

In the equation, $s_r = 0$ indicates that the r th transformer is in a normal state, $s_r = 1$ indicates that the r th transformer is in an extended fault state, and $s_r = 2$ indicates that the r th transformer is in a planned maintenance state.

However, due to the inherent uncertainty in the reliability parameters of substation components, the state probabilities P_N, P_M and P_s also exhibit uncertainty during sampling. If state probabilities were determined for each possible value of i in the component parameter correlation matrix and then simulated for each scenario, the computational load would become extraordinarily large, significantly impacting the speed of non-sequential Monte Carlo simulations. Drawing on the theory of extreme event sets, this paper applies the concept of extreme event sets to non-sequential Monte Carlo simulations. This approach enhances the speed of Monte Carlo simulations while accounting for the uncertainty in component parameters.

The extreme scenario set comprises the best-case and worst-case scenarios. The best-case scenario refers to the most favorable outcome for the risk assessment of the substation's main busbar configuration, while the worst-case scenario denotes the most unfavorable outcome. The probability envelope of component r 's normal state fluctuates within the interval $[P_N^{\min}, P_N^{\max}]$. The worst-case scenario occurs when $P_N = P_N^{\min}$ and the expanded state probability is $P_S + (P_N - P_N^{\min})$. State sampling adheres to the following principle:

$$s_r = \begin{cases} 0, & 0 \le R_r \le P_N^{\min} \\ 1, & P_N^{\min} < R_r \le P_S + (P_N - P_N^{\min}) \\ 2, & P_S + (P_N - P_N^{\min}) < R_r \le P_S + P_N + P_M \end{cases} \tag{8}$$

The optimal scenario occurs when $P_N = P_N^{\max}$ and the planned maintenance state probability is $P_M + (P_N^{\max} - P_N)$; state sampling adheres to the following principle:

$$s_r = \begin{cases} 0, & 0 \le R_r \le P_N^{\max} \\ 1, & P_N^{\max} < R_r \le P_S \\ 2, & P_S < R_r \le P_S + P_N + P_M \end{cases} \tag{9}$$

By conducting Monte Carlo simulations for both best-case and worst-case scenarios, the upper and lower bounds of fluctuations for each risk indicator can be obtained. Converting these risk indicator values into linkage coefficients enables the uncertainty of reliability parameters for main switching elements in substations to be reflected in the risk assessment results.

3.1.3 Substation Main Connection Risk Assessment Model

This paper assumes 100% reliability of the generating units. To analyze the impact of the substation main busbar configuration on the power grid, Monte Carlo sampling is performed on both the internal substation equipment and the grid components. The system state is obtained by integrating the results of both samplings. The risk assessment process for the substation main busbar configuration is illustrated in Figure 3.

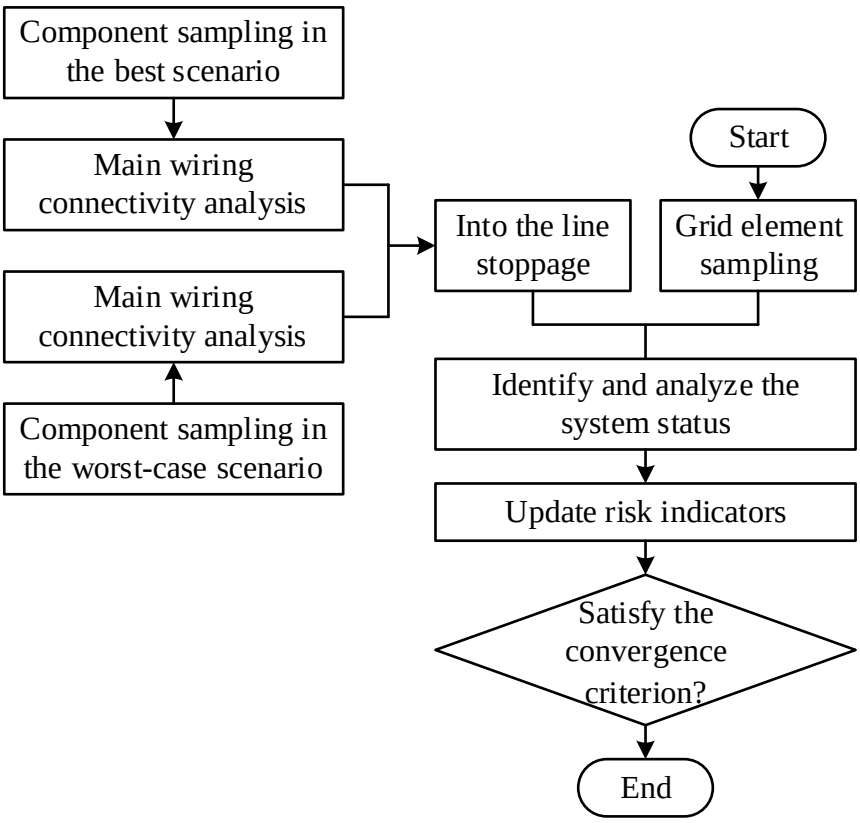

Figure 3: Flowchart of risk assessment for the main wiring of the substation

Step 1: Process the reliability parameters of components into connection coefficients.

Step 2: Perform Monte Carlo sampling on internal substation components under both best-case and worst-case scenarios. Compare the random numbers with the corresponding probability of equipment status within the station to determine whether it should be de-energized. For non-propagating faults, only the faulty component is de-energized; for propagating faults, both the faulty component and adjacent circuit breakers are de-energized.

Step 3: Analyze the connectivity of the substation's main busbar configuration under best-case and worst-case scenarios, outputting the set of deactivated incoming and outgoing lines.

Step 4: Sample grid components and merge these results with those from Step 3 to obtain the system-wide state sampling.

Step 5: Identify and analyze the system state. Utilize the improved optimal power flow method to determine the load shedding amount under the fault state.

Step 6: Calculate the risk metric based on the load shedding results. Determine whether the

Monte Carlo sampling meets the convergence criterion. If not, return to Step 2.

Step 7: Simulation concludes. Employ connectivity calculations to generate the risk metric results.

3.2 Comprehensive Evaluation Using Principal Component Analysis

Principal Component Analysis (PCA) is one of the most widely used data dimensionality reduction algorithms [28]. This method maps n-dimensional features onto a k-dimensional space, where the k dimensions represent entirely new orthogonal features (principal components) reconstructed from the original n features. By computing the covariance matrix of the data matrix, the eigenvalues and eigenvectors of the covariance matrix are obtained. The matrix is then formed by selecting the eigenvectors corresponding to the k largest eigenvalues (representing the largest variance). Collect the data to obtain the dataset X:

$$X = \{x_1, x_2, x_3, \cdots, x_n\} \tag{10}$$

Calculate the mean of the data sample for each indicator:

$$\overline{x} = \frac{1}{n}\sum_{i=1}^{n} x_i \tag{11}$$

Sample variance:

$$S^2 = \frac{1}{n}\sum_{i=1}^{n}(x_i - \overline{x})^2 \tag{12}$$

Then calculate the cross-covariance between two samples, such as the covariance between sample X and sample Y:

$$\begin{aligned} Cov(X,Y) &= E[(X - E(X))(Y - E(Y))] \\ &= \frac{1}{n}\sum_{i=1}^{n}(x_i - \overline{x})(y_i - \overline{y}) \end{aligned} \tag{13}$$

$Cov(X,X)$ represents the variance of a single dimension. When a sample contains n dimensional data indicators, the covariance is actually the covariance matrix Q. For example, the covariance of 3-dimensional data (X,Y,Z) is:

$$Q = Cov(X,Y,Z) = \begin{bmatrix} Cov(x,x) & Cov(x,y) & Cov(x,z) \\ Cov(y,z) & Cov(y,y) & Cov(y,z) \\ Cov(z,x) & Cov(z,y) & Cov(z,z) \end{bmatrix} \tag{14}$$

$$\lambda v = Qv \tag{15}$$

Using Equations (14) and (15), solve for the eigenvalues $\lambda_j = (j = 1,2,\cdots,n)$ and eigenvectors $v_j = (j = 1,2,\cdots,n)$ of the covariance matrix Q. Sort the eigenvectors by the magnitude of their eigenvalues to obtain a new eigenvector matrix W: $\lambda_a > \lambda_b > \lambda_c > \cdots$

$W = \{v_a, v_b, v_c, \cdots\}$.

The ACR of the sorted eigenvalues is calculated as follows:

$$ACR_k = \frac{\sum_{j=1}^{k} \lambda_j}{\sum_{j=1}^{n} \lambda_j} \tag{16}$$

Set the threshold Threshold. If $ACR \geq Threshold$, the number of principal components meeting the threshold is obtained. This achieves dimensionality reduction by replacing n indicator variables with k principal components. Subsequently, corresponding weights β are assigned to the reduced principal components. The weights β serve as coefficients in the multiple linear regression equation:

$$F = \beta_0 F_0 + \beta_1 F_1 + \cdots + \beta_k F_k \tag{17}$$

Solve for the comprehensive score of F after dimensionality reduction. Based on the magnitude of F, the optimal main busbar configuration for the 500kV substation can be determined.

4 Intelligent Generation and Evaluation of Main Connection Schemes for 500kV Substations

4.1 Experimental Results of 500kV Substation Main Connection Scheme Generation

Experiments were conducted using large language models, text embedding models, and TOP-K (number of relevant text matches) as variables. The large language models selected were GPT-3.5-Turbo and ChatGLM2-6B, while the text embedding models chosen were BGE-Large-ZH-v1.5 and Text2Vec-Base-Chinese. TOP-K refers to retrieving the top K most relevant solution texts from the local knowledge base during retrieval, with TOP-K values set to 1, 2, and 3 respectively. The Temperature parameter for large language models was set to 0, indicating minimal randomness in output generation. Evaluation metrics include BLEU, ROUGE-1, ROUGE-2, and ROUGE-L. Both BLEU and ROUGE metrics measure text overlap between generated and reference texts. ROUGE-1 assesses one-word phrase overlap, ROUGE-2 evaluates two-word phrase overlap, while ROUGE-L measures the length of the longest common subsequence, prioritizing preservation of original sequence and structure. BLEU, on the other hand, calculates the overlap for unigram, bigram, trigram, and tetragram phrases separately, then takes the average to assess the overall average overlap between generated and reference text phrases.

4.1.1 Overall Generation Effect Experiment of the Intelligent Generation Solution

The evaluation of 90 categories of 500kV substation main connection schemes is presented in Table 1, based on 10 groups of experiments involving 90 × 10 queries.

The experimental results indicate that for GPT-3.5-Turbo, text generation quality consistently improves as the TOP-K value increases. In contrast, ChatGLM2-6B achieves its highest text generation quality at a TOP-K value of 2. However, at TOP-K values of 2 or 3,

GPT-3.5-Turbo's performance surpasses that of ChatGLM2-6B. The maximum text length for a single 500kV substation main connection scheme reached 1,515 characters, with longer lengths observed at higher TOP-K values. This indicates that gpt3.5-turbo maintains high solution generation quality when processing larger prompts, while chatglm2-6b exhibits performance degradation under excessive prompts but still achieves high solution generation accuracy.

Table 1: The main connection scheme text is the overall generation evaluation

Big language model	Text embedded model	TOP-K	BLEU	ROUGE-1	ROUGE-2	ROUGE-L
gpt3.5-turbo	Bge-large-zh-v1.5	1	0.8474	0.934	0.9123	0.929
		2	0.8811	0.9708	0.9577	0.9698
		3	**0.9128**	**0.9875**	**0.9778**	**0.9879**
	Text2vec-base-chinese	1	0.8005	0.8861	0.8661	0.8814
		2	0.857	0.9324	0.9191	0.9316
		3	**0.8708**	**0.9647**	**0.9507**	**0.9645**
chatglm2-6b	Bge-large-zh-v1.5	1	0.8497	0.9384	0.9122	0.9308
		2	**0.862**	**0.9567**	**0.9358**	**0.9561**
		3	0.812	0.9337	9.9033	0.9298
	Text2vec-base-chinese	1	0.8053	0.9031	0.864	0.893
		2	**0.8409**	**0.9494**	**0.9232**	**0.9445**
		3	0.8137	0.9222	0.8858	0.9118

4.1.2 Experiment on the Accuracy of Disposal Plan Generation

To further investigate the impact of TOP-K on the accuracy of large language model responses under conditions of accurate retrieval by text embedding models, we excluded the 500kV substation main connection schemes with previous retrieval errors and re-evaluated the performance of large language models under fully accurate retrieval conditions. The evaluation of text generation accuracy for 500kV substation main wiring schemes is shown in Table 2. Results indicate that for GPT-3.5-Turbo, TOP-K values ranging from 1 to 3 did not significantly affect response accuracy. This further confirms GPT-3.5-Turbo's robust adaptability when processing multiple text inputs. However, for ChatGLM2-6B, smaller TOP-K values yield higher response accuracy. Large language models trained on the 500kV substation main wiring scheme knowledge base demonstrate outstanding performance in long-text generation, achieving a maximum ROUGE-L score of 0.9876.

Table 2: The main connection scheme text generation accuracy evaluation

Big language model	Text embedded model	TOP-K	BLEU	ROUGE-1	ROUGE-2	ROUGE-L
gpt3.5-turbo	Bge-large-zh-v1.5	1	0.9153	0.9819	0.9714	0.9807
		2	0.9005	0.9859	0.9733	0.9842
		3	0.912	0.987	0.9783	**0.9876**
	Text2vec-base-chinese	1	0.9092	0.9843	0.9744	0.9842
		2	0.9089	0.9836	0.9733	0.9831
		3	0.8883	0.9797	0.9663	0.9801
chatglm2-6b	Bge-large-zh-v1.5	1	**0.9171**	**0.9786**	**0.9661**	**0.9778**
		2	0.8775	0.9644	0.9472	0.9649
		3	0.8117	0.9348	0.9034	0.9295
	Text2vec-base-chinese	1	**0.9116**	**0.9754**	**0.964**	**0.9753**
		2	0.8835	0.9732	0.9594	0.9734
		3	0.8312	0.9323	0.9011	0.9233

4.2 Operational Risk Assessment of the Main Busbar Configuration at the 500kV Substation

This paper presents a risk assessment method for substation main wiring configurations implemented via Matlab programming. The analysis focuses on two representative substations: the one at BUS2 in the IEEE-RBTS system and the one at BUS18 in the IEEE-RTS96 system. The electrical main busbar system topologies of the substations are shown in Figures 4(a) and (b), respectively. Figure 4(a) depicts an end substation responsible for supplying power to the downstream distribution system. Its electrical main busbar adopts a single-busbar configuration with two incoming lines, G1 and G2, serving as substation power sources. These lines supply power to four load points, P1 to P4, with a combined peak load of 30 MW. Figure 4(b) depicts a hub substation, which aggregates and distributes electrical energy while supplying power to downstream grid loads. The substation is powered by three incoming lines G1 to G3. P2 is an outgoing load point, while P1 represents a downstream grid load point. The combined peak load of P1 and P2 is 525 MW, with a uniform power factor of 0.99 considered for all loads.

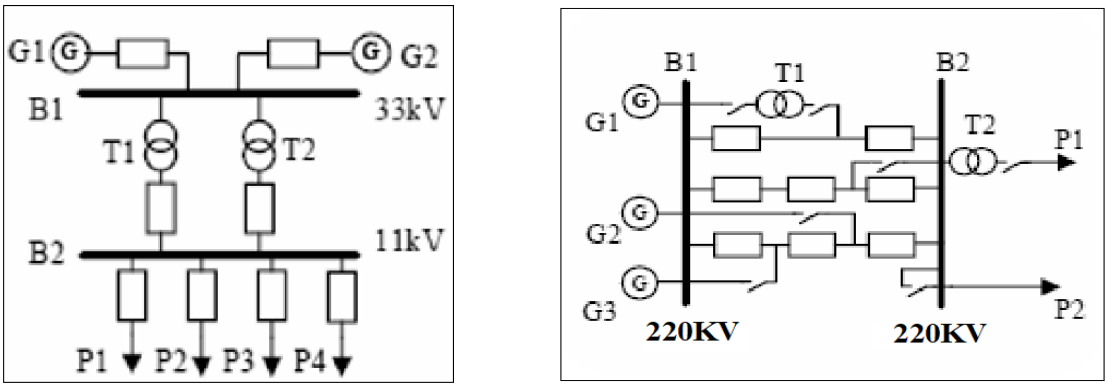

(a) IEEE-RBTS BUS2 (b) IEEE-RTS96 BUS18

Figure 4: Schematic Diagram of the Example System

Based on the proposed equivalent method for variable-capacity networks in electrical main wiring diagrams, the electrical main wiring shown in the figure above is first converted into an equivalent capacity graph G. Since this study focuses on operational risks in electrical main wiring, it is assumed that substation power supplies are fully reliable—meaning no load losses will occur due to insufficient power supply.

4.2.1 Model Validity Verification

To validate the effectiveness of the proposed algorithm, three models were employed to calculate risk indicators for the test system, with the evaluation objective being the power loss risk at any load point.

Model 1: A conventional electrical main wiring risk assessment model using connectivity loss as the fault discrimination criterion. The fault discrimination model employs the reachability matrix from conventional assessments for connectivity determination.

Model 2: This paper proposes a risk assessment model based on set pair analysis, but utilizes conventional methods for maximum flow calculation in main wiring transmission capacity computation.

Model 3: This paper proposes a risk assessment model based on set pair analysis, employing an improved optimal power flow algorithm for maximum flow calculation. Since the conventional electrical main busbar risk assessment in Model 1 uses connectivity as the sole

fault criterion without accounting for equipment load capacity, all equipment capacities in Models 2 and 3 are temporarily set to ∞ for comparative risk metric calculations. This equates to load shedding occurring only when faults cause connectivity loss in the main busbar.

For the two example systems shown in Figure 4, load demands were set to their respective peak values, the assessment period T was set to 1 year, and the variance coefficient convergence condition for risk indicators was set to ε=0.04. The calculated risk indicator results for both systems are presented in Tables 3 and 4, respectively. As shown in the tables, when disregarding equipment load capacity, the three risk metrics of Model 3 are numerically consistent with those of Model 1. Minor discrepancies in metric values stem from sampling randomness, validating the accuracy of the proposed method. Additionally, for the IEEE-RBTS BUS2 system, Model 1 exhibits the shortest computation time, followed by Model 3 based on the improved optimal power flow method, while Model 2 using the conventional algorithm requires the most computational resources. This is because Model 1 performs fault consequence analysis solely through the reachability matrix method, utilizing simple matrix multiplication and addition to determine connectivity between given nodes and iterate risk indicator calculations. whereas Models 2 and 3 require iterative generation of hierarchical residual networks based on optimal power flow algorithms to compute maximum flows in substation networks, consuming more computational resources. However, Model 3 achieves approximately three times faster computation than Model 2. For the IEEE-RTS96 BUS18 system, since the equivalent edges of the two transformers do not meet the requirements of the improved optimal power flow algorithm, iterative calculations of the residual network are still necessary. Therefore, Models 2 and 3 exhibit nearly identical computational times while ensuring consistent accuracy of the results.

Table 3: Comparison of Risk Indicator Calculation Results for the IEEE-RBTS System

Method	PLC (%)	EFLC	EENS (MWh/year)	Time (s)
Model 1	0.004555	0.0452	2.1245	2.12
Model 2	0.004578	0.0455	2.0889	12.22
Model 3	0.004523	0.0471	2.0578	4.15

Table 4: Comparison of Risk Indicator Calculation Results for the IEEE-RTS96 System

Method	PLC (%)	EFLC	EENS (MWh/year)	Time (s)
Model 1	0.001888	0.02062	8556.3535	2.98
Model 2	0.001858	0.02008	8488.3366	17.12
Model 3	0.001956	0.02068	8618.8872	16.98

Based on the above calculations and considering the constraint of equipment rated capacity, the electrical main switchgear risk index accounting for equipment load capacity can be derived. Using the IEEE-RTS BUS18 substation as an example again, under identical calculation conditions, the convergence of its risk index and the calculation results are shown in Figures 5 and 6, respectively. As shown in the figures, after approximately 4000 independent samples, the variance coefficients of all risk indicators are below the specified threshold ε=0.04, indicating convergence. Among them, η (EENS) exhibits the slowest convergence rate and is thus suitable as the termination criterion for calculations. Regarding the risk indicator calculation results, after accounting for equipment load capacity, PLC is 0.0626%, representing an increase of approximately 29.5 times compared to calculations without load capacity consideration. Similarly, EFLC is 0.4671 times/year, increasing by about 20 times, while EENS is 7.3521×10^4 MWh, increasing by approximately 7.98 times.

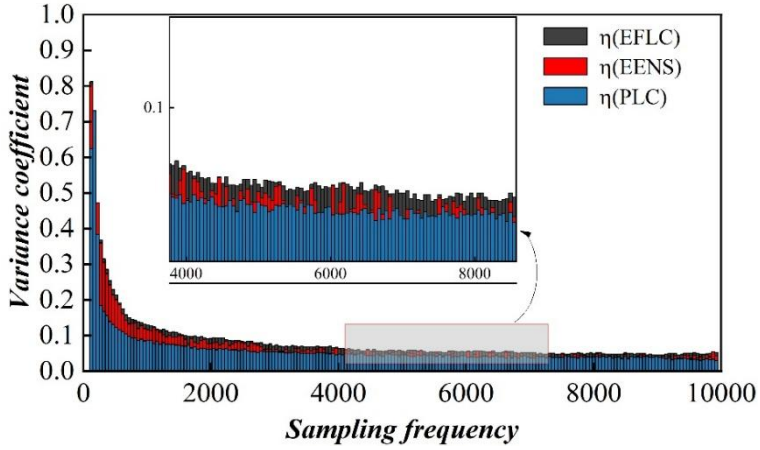

Figure 5: Variation of the Variance Coefficient for Operational Risk Indicators

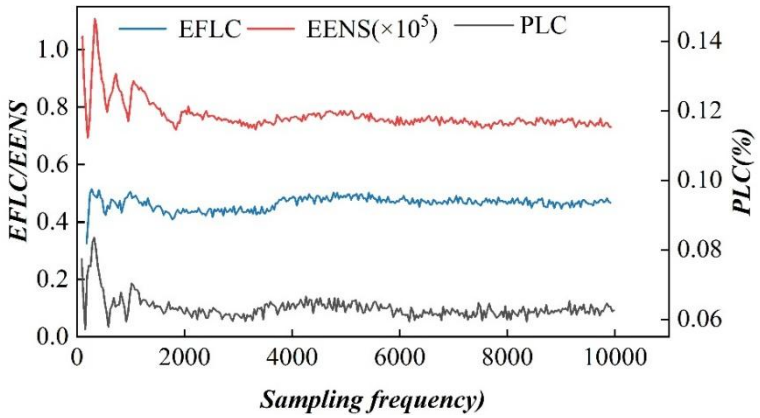

Figure 6: The Iterative Convergence Process of Operational Risk Indicators

4.2.2 Dynamic Operational Risk Assessment of Substation Main Connections

Leveraging the sequential Monte Carlo sampling technique proposed in this paper, which preserves temporal operational characteristics, and combining it with an improved maximum power flow calculation method, enables dynamic operational risk assessment of electrical main switchgear configurations while accounting for equipment load capacity.

Using the IEEE-RTS BUS18 substation as the study subject again, the variation of risk indicators over one year is shown in Figure 7. The operational risk indicators exhibit a close correlation with the substation's load level changes over the year, though this relationship is nonlinear. When load levels exceed 420 MVA, all risk indicators surge sharply. This occurs because, below this threshold, only faults of second-order or higher affecting system connectivity cause load loss. Above this threshold, however, a fault disconnecting load point P2 from its power source requires load point P1 to shed more than T2 capacity to prevent equipment overload. Furthermore, from an annual timing perspective, operational risks are relatively lower between days 55 and 110, and between days 250 and 290. This indicates that for this system, the operational risks associated with the main electrical busbar configuration during spring and autumn are significantly lower than those during summer and winter.

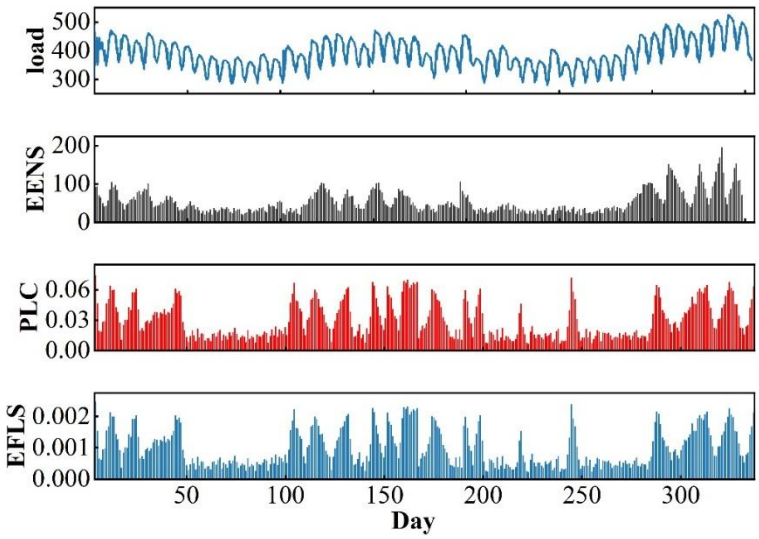

Figure 7: The Variation of Dynamic Operational Risk Indicator

Changes in risk indicators based on conventional assessment methods are shown in Figure 8. Since these methods cannot account for the impact of equipment load capacity on risk indicators, neither the PLC nor EFLC indicators are affected regardless of load variations within a year. In contrast, the EENS indicator exhibits a largely linear relationship with load. This occurs because conventional calculations relate solely to the electrical main wiring configuration and are independent of operational conditions.

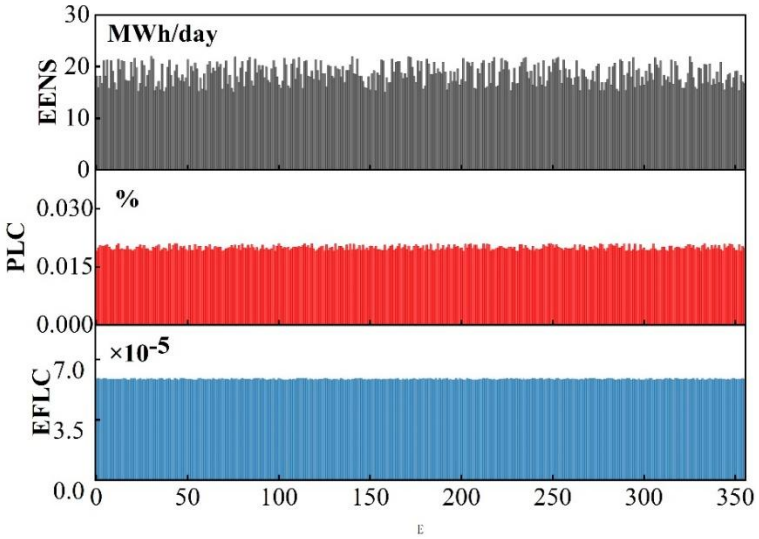

Figure 8: The Variation of Risk Indicators Based on Conventional Assessment Methods

4.3 Comprehensive Evaluation

This section evaluates and selects comprehensive solutions for safety, efficiency, and cost using the 500kV smart substation design scheme generated by this paper's algorithm. The scheme features outdoor AIS and conventional outdoor GIS configurations on the 220kV side. The evaluation compares the two design options described in the principal component analysis (PCA) assessment model. Initial values for model calculations required to evaluate next-generation smart substation design schemes using the PCA assessment model are shown in Table 5. In accordance with the State Grid Corporation of China's Guidelines for Design Service

Life of Transmission and Transformation Projects (Trial), the mean time between failures (MTBF) for all primary substation equipment types applied in this study is assumed to be 40 years. Thus, the total life cycle T is set to 40 years, with an annual interest rate i of 8%.

Table 5: Evaluation model initial value

	Numerical value		Unit
	AIS	GIS	
Primary cost	11222	10918	10000 yuan
Maintenance cost	75.575	58.885	10000 yuan
Reliability	0.998812	0.999901	--
Failure rate	0.551234	0.363636	Annual
No load loss	0.08	0.08	%
Load loss	0.33	0.33	%
Electrovalence	0.48	0.48	Yuan/kwh

This paper employs computer simulation to perform sampling of random variables using simple sampling methods. The sampling frequency is set at 4000 times. The specific sampling results for the Poisson distribution are shown in Figure 9. As illustrated, when the sampling frequency reaches 4000 times, the bar chart of the simulated random variable results approximates the probability density function of the Poisson distribution. Therefore, a sampling frequency of 4000 times meets the expected requirements.

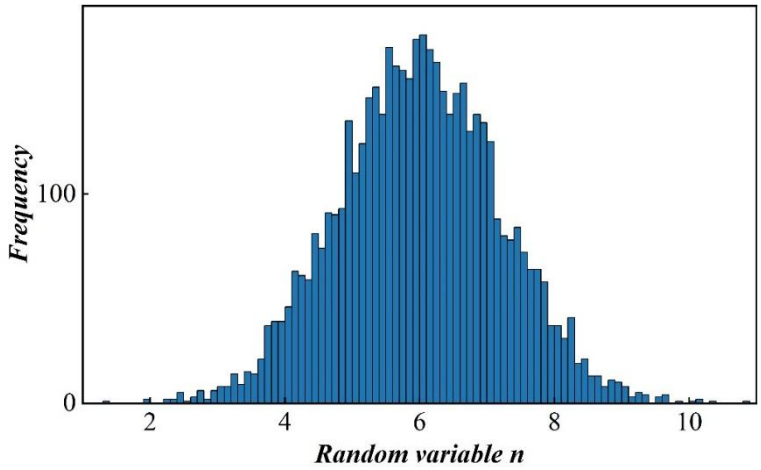

Figure 9: The results of the distribution of the body poisson

Figure 10 illustrates the relationship between the number of simulations and the comprehensive evaluation value of the principal component analysis method. The figure reveals that when the simulation count reaches approximately 4000 iterations, the AIS scheme converges to an improved SEC indicator value of 6.18, while the GIS scheme converges to 3.61. This demonstrates the excellent convergence properties of the proposed algorithm. Furthermore, the outdoor GIS scheme generated using a large language model proves to be the superior solution for the distribution equipment of this 500kV substation.

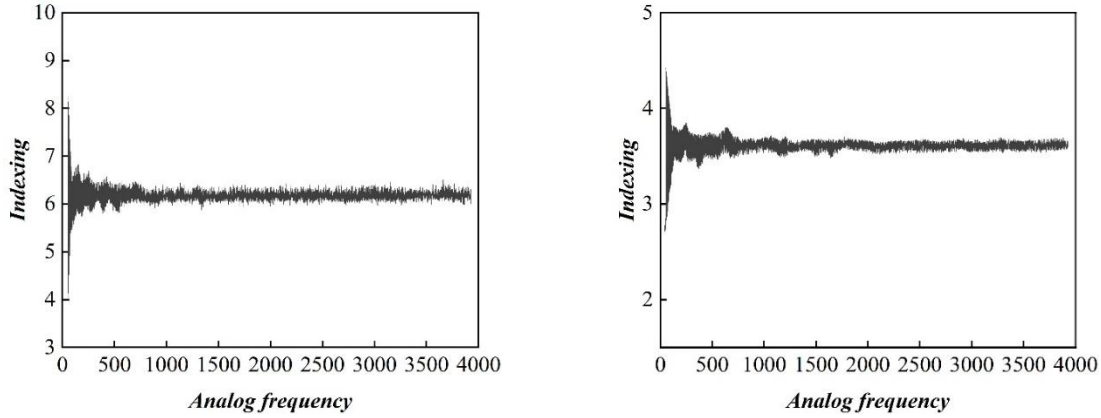

(a) AIS (b) GIS

Figure 10: The relationship between the simulation number and the evaluation value

Figure 11 shows the probability distribution of the improved principal component analysis (PCA) indicator values for both schemes when the simulation count is 4000. Figure 12 shows the cumulative probability distribution of the improved PCA indicator values for both schemes when the simulation count is 4000. From these two figures, it can be observed that in the design of this 500kV next-generation smart substation, when using AIS distribution equipment and outdoor GIS distribution equipment respectively, their corresponding improved principal component analysis target values follow Poisson distributions with mean values of 6.18 and 3.61, respectively. This theoretically demonstrates that the outdoor GIS scheme is superior. The primary reasons for this phenomenon are analyzed as follows:

(1) In the analysis, the mean distribution of accident occurrence frequency is determined by the failure rate of the design scheme. The inclusion of operational risk as a sub-indicator within the cost metric comprehensively considers the interplay between technical feasibility, safety, and economic viability. This results in the principal component analysis composite indicator value for the GIS design scheme being lower than that of the AIS distribution scheme.

(2) By determining coefficient values for various indicators through PCA, the comprehensive evaluation model increased the coefficients for reliability benefit and safety indicators while reducing the coefficient for initial investment cost. Consequently, the GIS indicator value further decreased relative to the AIS indicator value. In practice, for design solutions, safe and reliable operation is the prerequisite for ensuring economic viability. Therefore, assigning higher weights to reliability benefit and safety indicators than to investment cost indicators is reasonable.

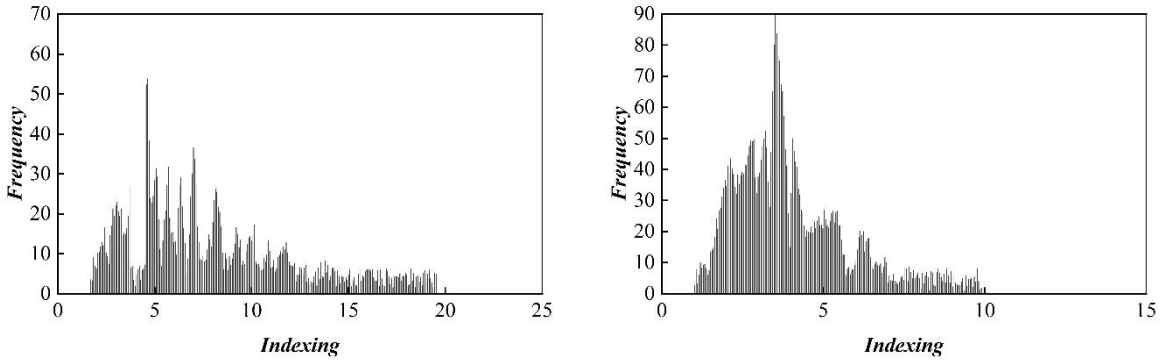

(a) AIS (b) GIS

Figure 11: The probability distribution of the index

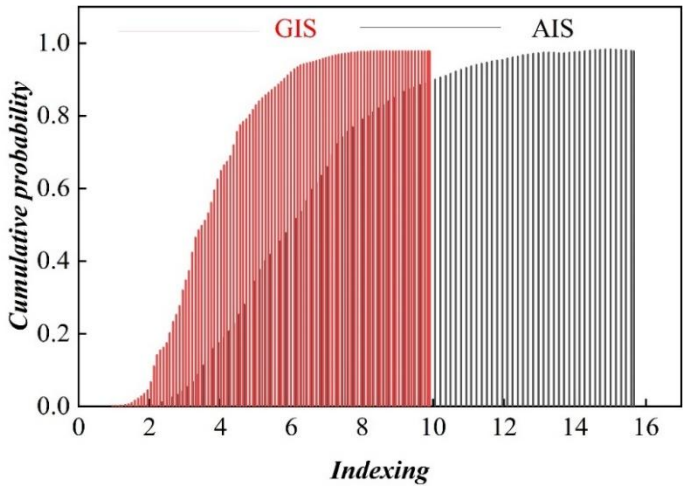

Figure 12: The cumulative probability distribution of the index

5 Conclusion

To address the issues of inefficiency and high complexity in the current design of main busbar schemes for 500kV substations, this paper designs and implements a vector retrieval-enhanced intelligent design support system for 500kV substation main busbar schemes based on large language models. Comprehensive evaluation demonstrates that the proposed method offers the following advantages:

(1) Accuracy: Demonstrates excellent long-text generation accuracy for 500kV substation main busbar schemes, achieving a maximum ROUGE-L score of 0.9876. Even with the small-parameter large language model ChatGLM2-6B, ROUGE-L reaches 0.9561, maintaining high performance.

(2) Efficiency: By refining 500kV substation main wiring scheme solutions, it addresses the issue of unclear outputs from large language models, enhancing decision-making efficiency.

(3) Utilizing the IEEE-RBTS and IEEE-RTS96 test case systems, the effectiveness and advanced nature of this method were validated. Results indicate that changes in load levels during operation significantly impact the operational risks of electrical main wiring. The proposed method assists operators in understanding the patterns of operational risk changes in substations.

Since generic text embedding models and retrieval methods can compromise the quality of generated response plan texts, future research should focus on developing specialized text embedding models and redesigning retrieval methods as potential approaches to further enhance text generation quality.

Funding

Project Supported by Science and Technology Project of State Grid under Grant No. 5200-202356472A-3-2-ZN.

About the Author

Yuwei Li was born in Jining, Shandong, P.R. China, in 1996. She received her master’s degree from Xi’an Jiaotong University, Xi’an, P.R. China. Currently, she works at the Economic &

Technology Research Institute of State Grid Shandong Electric Power Company, Jinan, P.R. China, where her research focuses on the intelligent design of power transmission and transformation systems.

Jinghe Zhang was born in Jinan, Shandong, P.R. China, in 1986. She received her master's degree from Shandong University, Jinan, P.R. China. Currently, she works at the Economic & Technology Research Institute of State Grid Shandong Electric Power Company, Jinan, P.R. China, where her research focuses on the intelligent design of power transmission and transformation systems.

Feng Lan was born in Jining, Shandong, P.R. China, in 1986. He received his master's degree from Shandong University, Jinan, P.R. China. Currently, he works at the Economic & Technology Research Institute of State Grid Shandong Electric Power Company, Jinan, P.R. China, where his research focuses on the intelligent design of power transmission and transformation systems.

Mingshu Zhao was born in Aba, Sichuan, P.R. China, in 1990. He received his master's degree from Tsinghua University, Beijing, P.R. China. Currently, he works at the Sichuan Energy Internet Research Institute of Tsinghua University, Chengdu, P.R. China, where his research focuses on the applications of large language model and computer vision methods for smart grid system.

Yi Luo was born in Chengdu, Sichuan, P.R. China, in 1987. He received his PhD from the University of Edinburgh, United Kingdom. Currently, he works at the Sichuan Energy Internet Research Institute of Tsinghua University, Chengdu, P.R. China, where his research focuses on artificial intelligence and cloud computing applications in power systems.

References

[1] Farooq, H., Ali, W., Iqbal, H., Rasool, A., Sajjad, I. A., & Noon, A. A. (2021). Evaluation of the safety performance of a 500-kv ac substation grounding using ieee standard 80-2013. Electrica, 21(2), 225-234.

[2] He, Y., Guo, Y., Kuang, J., Li, G., Wang, C., Ding, Z., ... & Tan, L. (2019, April). Application Research on General Equipment of 35-750kV Substation of State Grid Corporation in China. In 2019 2nd International Conference on Electrical Materials and Power Equipment (ICEMPE) (pp. 652-657). IEEE.

[3] Zhang, T., Li, Y., Xu, L., Su, G., Liu, Q., & Xiong, Z. (2024, April). Study on Optimization and Application of 500kV HGIS Layout. In 2024 9th Asia Conference on Power and Electrical Engineering (ACPEE) (pp. 2489-2493). IEEE.

[4] Zhou, Y., Huang, Y., He, L., Luo, Z., & Su, S. (2024, December). Analysis of ground leakage issues due to incorrect wiring in low voltage distribution substation area. In 4th Energy Conversion and Economics Annual Forum (ECE Forum 2024) (Vol. 2024, pp. 1051-1056). IET.

[5] Piesciorovsky, E. C., Borges Hink, R., Werth, A., Hahn, G., Lee, A., & Polsky, Y. (2023). Assessment and commissioning of electrical substation grid testbed with a real-time simulator and protective relays/power meters in the loop. Energies, 16(11), 4407.

[6] Gryzlov, A. A., & Grigor'Ev, M. A. (2018). Improving the reliability of relay-protection and automatic systems of electric-power stations and substations. Russian Electrical Engineering, 89(4), 245-248.

[7] Van Hertem, D., Leterme, W., Chaffey, G., Abedrabbo, M., Wang, M., Zerihun, F., & Barnes, M. (2019). Substations for future HVDC grids: Equipment and configurations for connection of HVDC network elements. IEEE Power and Energy Magazine, 17(4), 56-66.

[8] Shuang, S., Xingjin, Q., Qiangsheng, B., Yi, Y., & Liangliang, S. (2017). Research on technical scheme of outdoor-layout relay protection in smart substation. The Journal of Engineering, 2017(13), 1215-1219.

[9] Yang, H., Zhang, K., & Tang, A. (2022). Risk assessment of main electrical connection in substation with regional grid safety constraints. Ieee Access, 10, 27750-27758.

[10] Smail, H., Alkama, R., & Medjdoub, A. (2018). Optimal design of the electric connection of a wind farm. Energy, 165, 972-983.

[11] Wang, N., Li, Y., Yang, H., Hu, Y., & Wang, S. (2020). Research on Reliability Evaluation and Scheme Optimization of Main Connection Mode of Substation. In E3S Web of Conferences (Vol. 185, p. 01002). EDP Sciences.

[12] Panova, E. A., Varganova, A. V., & Sorokin, N. S. (2019, October). The algorithm for automated development of design drawings of one-line diagrams of distribution devices for 6-10 kV of substations. In 2019 International Multi-Conference on Industrial Engineering and Modern Technologies (FarEastCon) (pp. 1-5). IEEE.

[13] Zhang, L., Zhao, L., Sun, P., Zhang, L., & Tian, G. (2017, November). An automatic layout algorithm of main wiring diagram of substation based on improved simulated annealing algorithm. In 2017 4th International Conference on Systems and Informatics (ICSAI) (pp. 312-317). IEEE.

[14] Peng, Z., Yan, G., Zhongshan, Q., Huiyong, L., Mouying, L., & Shengnan, L. (2020, August). CIM/G graphics automatic generation in substation primary wiring diagram based on image recognition. In Journal of Physics: Conference Series (Vol. 1617, No. 1, p. 012007). IOP Publishing.

[15] Qiu, J., Li, B., Wang, A., & Hao, N. (2024, June). The Graph Aided Generation System in Substation Based on Style. In International Conference on Internet of Things, Communication and Intelligent Technology (pp. 131-144). Singapore: Springer Nature Singapore.

[16] Yang, D., You, H., Zhang, Y., Ren, X., Lu, B., Jin, J., ... & Jin, D. (2024, May). Identification of Primary Wiring Diagram in Substation Based on YOLOv5. In 2024 IEEE 2nd International Conference on Power Science and Technology (ICPST) (pp. 603-609). IEEE.

[17] Chen, T., Li, H., Cao, Y., & Zhang, Z. (2023). Substation Operation Sequence Inference Model Based on Deep Reinforcement Learning. Applied Sciences, 13(13), 7360.

[18] Zhao, H., Chen, H., Yang, F., Liu, N., Deng, H., Cai, H., ... & Du, M. (2024). Explainability for large language models: A survey. ACM Transactions on Intelligent Systems and Technology, 15(2), 1-38.

[19] Zubiaga, A. (2024). Natural language processing in the era of large language models. Frontiers in artificial intelligence, 6, 1350306.

[20] Liu, J., Xia, C. S., Wang, Y., & Zhang, L. (2023). Is your code generated by chatgpt really correct? rigorous evaluation of large language models for code generation. Advances in Neural Information Processing Systems, 36, 21558-21572.

[21] Ibrahim, N., & Kashef, R. (2025). Exploring the emerging role of large language models in smart grid cybersecurity: a survey of attacks, detection mechanisms, and mitigation strategies. Frontiers in Energy Research, 13, 1531655.

[22] Pathan, M. K. (2025). Investigating the Efficacy of Multimodal Large Language Models in Cross-Domain Knowledge Transfer. Journal of Artificial Intelligence, 3, 100009.

[23] Gill, J. K., Chetty, M., Lim, S., & Hallinan, J. (2024). Large language model based framework for automated extraction of genetic interactions from unstructured data. Plos one, 19(5), e0303231.

[24] Shi, H., Fang, L., Chen, X., Gu, C., Ma, K., Zhang, X., ... & Lim, E. G. (2024). Review of the opportunities and challenges to accelerate mass-scale application of smart grids with large-language models. IET Smart Grid, 7(6), 737-759.

[25] Gao, Q., Shen, L., Shi, J., Gu, X., Gu, S., Ge, Y., ... & Ji, J. (2025). Transformer-Enhanced Intelligent Microgrid Self-Healing: Integrating Large Language Models and Adaptive Optimization for Real-Time Fault Detection and Recovery. Energy Engineering: Journal of the Association of Energy Engineers, 122(7), 2767.

[26] Song, Y., Yan, H., Sun, C., & Huang, J. (2024, November). An LLM-Assisted Framework for Synthetic Power Network Graph Generation. In 2024 IEEE 7th Student Conference on Electric Machines and Systems (SCEMS) (pp. 1-6). IEEE.

[27] Xu Li, Chunlin Gong, Liangxian Gu, Zhao Jing, Hai Fang & Ruichao Gao. (2019). A reliability-based optimization method using sequential surrogate model and Monte Carlo simulation. Structural and Multidisciplinary Optimization,59(2),439-460.

[28] Lyes Rabhi, Abdelkader Lemou, Riad Ladji, Nicolas Bonnaire, Jean Sciare & Noureddine Yassaa. (2025). Source apportionment of PM2.5 in a coastal City of Algeria using principal component analysis model. Journal of Atmospheric Chemistry,82(2),13-13.